Cite this article
Paradeisiotis A and Stagonas D
Reproduction of critical wave events for the design of floating offshore structures.
Maritime Engineering,
https://doi.org/10.1680/jmaen.26.00005

Research Article
Paper 2600005
Received 09/01/2026; Accepted 09/05/2026

Maritime Engineering

Reproduction of critical wave events for the design of floating offshore structures

Andreas Paradeisiotis
Department of Civil and Environmental Engineering, University of Cyprus, Nicosia, Cyprus (Orcid:0000-0001-6939-726X) (corresponding author: aparad01@ucy.ac.cy)

Dimitris Stagonas
Department of Civil and Environmental Engineering, University of Cyprus, Nicosia, Cyprus (Orcid:0000-0002-2010-2659)

This work presents a methodology for identifying and reproducing critical wave events that induce extreme mooring line tension in floating offshore wind turbines. The approach begins with fully non-linear sea-state realisations, generated using a JONSWAP spectrum and propagated via a fully non-linear potential flow solver. The Hilbert transform is applied on the linear component obtained from a four-wave spectral decomposition process of the surface elevation, to extract amplitude envelopes and instantaneous phase information, enabling the isolation of critical wave events responsible for extreme structural responses. Each critical wave event is expressed as a sum of focused wave groups using a Gaussian envelope regression methodology, allowing for individual iterative amplitude correction and phase focusing to overcome the challenges of reproducing steep wave events. The corrected focused wave groups are then recombined to create a 'Hyper-Group' with accurate spatial and temporal focusing at the desired location. The reproduced event is numerically validated against the original sea-state, demonstrating very good agreement in induced mooring line tension. This methodology provides an efficient framework for generating realistic design waves, supporting targeted numerical and experimental testing of floating offshore wind turbines under extreme conditions.

Keywords: design waves/focused wave groups/offshore engineering/UN SDG 7: Affordable and clean energy/waves & wave loading

1. Introduction

A design wave is a representative wave profile or episode used in the structural and hydrodynamic analysis of offshore and marine structures to assess their performance under extreme environmental conditions. Unlike fully random sea states, which require lengthy time-domain simulations, design waves are typically short-duration, deterministic, or response-conditioned wave (RCW) profiles that capture the essential characteristics of extreme events. Their purpose is to simplify the evaluation of ultimate loads, motions, and structural integrity while ensuring safety and reliability. Design waves are particularly valuable in the early stages of design, where rapid iteration and comparative analysis are critical, as well as in detailed assessments where computational efficiency is paramount.

Offshore structures, such as floating wind turbines, must withstand rare but severe wave events that can induce critical loads and responses. Traditional approaches relying on irregular sea state simulations – though comprehensive – are often computationally expensive and time-consuming. Design waves address this challenge by distilling the most severe wave conditions into manageable, repeatable profiles that can be analysed using deterministic or simplified methods. These waves are derived from statistical analyses, probabilistic models, or response-conditioned techniques, ensuring they represent the most probable extreme events for a given return period or environmental condition.

In industry practice, design waves are integrated into design standards and guidelines issued by classification societies and regulatory bodies. For example, DNV (Det Norske Veritas) and ABS (American Bureau of Shipping) provide frameworks for using design waves in the structural assessment of offshore installations in documents like American Bureau of Shipping (2020); Palfy (2016). Standards, such as DNV GL AS (2021) and DNV GL (2018), recommend the use of design waves for ultimate limit state and fatigue limit state assessments, often allowing for the application of deterministic design waves (e.g. NewWave, Stokes waves) or RCWs to evaluate extreme loads, provided calibration against fully random sea state simulations or experimental data.

The NewWave deterministic model for extreme wave crests in random seas introduced by Tromans *et al*. (1991) separates the wave surface displacement into random and deterministic components. This 'most probable extreme wave' model offered a computationally efficient alternative to time-domain simulations and was further explored by Bennett *et al*. (2012), Whittaker *et al*. (2016), and Hann *et al*. (2018) among others, emerging as a central tool for modelling abnormal or focused wave groups (FWGs). However, as shown by Hann *et al*. (2018), while the NewWave can model extreme responses, its effectiveness depends on the inclusion of background wave trains and the consideration of non-linear wave–wave interactions, which could limit its predictive accuracy.

Taylor *et al*. (1997) and Cassidy *et al*. (2001) introduced the concept of the Constrained NewWave (CNW) to address the need for dynamic assessment models that account for structural, foundation, and wave loading non-linearities. Constraining deterministic NewWaves within random backgrounds highlights the importance of random wave histories in extreme response statistics. This approach builds on the work of Lindgren (1970), where the key idea is to constrain the random process such that it includes a specified extreme event at a particular time, while the rest of the process remains statistically consistent with the underlying random sea state.

In parallel, design wave methodologies increasingly focused on response-conditioned approaches, aiming to capture the most critical wave episodes that induce extreme structural responses, an example being the conditional random response wave methodology by Skjoldager Dietz (2005). Brown *et al*. (2023) and Hou and Liu (2024) explored the use of short design waves and CNW methods to reduce computational costs while targeting extreme responses. Short design waves showed potential for predicting surge and heave extremes in semi-submersible platforms, but required refinement for pitch predictions. Dermatis *et al*. (2025) introduced an approach for RCWs, accounting for combined wave- and low-frequency responses in moored floating bodies. By using both response amplitude operators and quadratic transfer functions (QTFs), short-duration wave episodes exciting resonant slow-drift motions were identified and validated the approach experimentally.

Such methods represent a shift from purely statistical or deterministic design waves to explicitly accounting for the dynamic wave-structure interaction, offering more realistic and targeted assessments of extreme loads. The conceptual framework is that extreme structural responses are often triggered by specific wave characteristics, such as wave grouping, phase alignment, or resonant interactions. Wave groups are particularly consequential for floating offshore structures by inducing resonant motions, extreme loads, and non-linear responses, while they can also excite low-frequency (slow-drift) motions. Aliyar *et al*. (2025) showed that FWGs, especially with directional spreading, amplify odd and even harmonic responses in surge and pitch, leading to coupled resonant behaviours. In addition, wave groups often culminate in breaking waves, which pose severe threats to structures. Moreover, Tang *et al*. (2019) observed that wave groups exhibit asymmetry and envelope contraction due to non-linearities, affecting the harmonic content of structural responses.

Several methods are employed for identifying wave groups in surface elevation time histories. The Hilbert transform is widely used to extract the wave envelope, which is then analysed for group characteristics. Hudspeth and Medina (1988) compared Hilbert envelopes with the smoothed instantaneous wave energy history introduced by Funke and Mansard (1979), showing that the Hilbert transform effectively captures group lengths and frequencies. Senthilkumar *et al*. (2015) applied the Hilbert-Huang transform of Huang *et al*. (1999) to decompose wave groups in crossing seas, using intrinsic mode functions to identify groupiness factors. In addition, Fu *et al*. (2021) proposed a wavelet-based detector to identify wave groups and predict freak waves, where the time-frequency localisation is ideal for detecting transient group events and their non-linear evolution.

In experimental settings, the phase-inversion (harmonic separation) method is used to separate harmonic components. Fitzgerald *et al*. (2014) and Adcock *et al*. (2019) developed phase-based harmonic separation techniques, using multi-phase signals to extract odd and even harmonics. Harmonic decomposition allows for the separation of bound and free waves, improving the accuracy of group analysis. This method is particularly effective for FWGs, where non-linearities are localised. A more recent development of a four-phase method can be seen in Liu *et al*. (2025).

Hansen *et al*. (2025) provided further experimental insights into the use of design waves for floating wind turbines. Harmonic separation revealed that even harmonic responses dominate total surge and pitch responses, while design waves targeting maximum responses in surge and pitch were validated, even though harmonic low-frequency surge responses remained challenging to reproduce accurately. Furthermore, drift motions have been experimentally demonstrated to be associated with sub-harmonic components. Gudmestad *et al*. (2009) linked ringing and springing responses in floating structures to sub-harmonic resonance, where difference-frequency loads excite low-frequency motions. Extended phase manipulation is employed to reconstruct missing phases and separate weakly non-linear effects from strong non-linearities. Stagonas *et al*. (2018) and Buldakov *et al*. (2017) used iterative focusing techniques to generate wave groups with controlled spectra, enabling the study of extreme responses in laboratory and numerical settings.

In previous work, Stagonas and Paradeisiotis (2025) introduced a methodology for envelope regression of critical wave events (CWEs) and their reconstruction as a superposition of FWGs, termed a 'Hyper-Group' (HG). This methodology is designed for the systematic processing of large numbers of CWEs, by describing each one as a collection of Gaussian functions (elementary envelopes) and certain frequency and phase related scalar parameters. This process has been used to develop a probabilistic framework for generating Design Hyper-Groups (DHGs).

To clarify the objectives of this work and the rationale behind the demonstration approach, the following key terms must first be defined: 'Critical Wave Event', 'Hyper-Group' and 'Design Hyper-Group'.

Critical wave event: A short-duration segment of a sea-state surface elevation that induces extreme structural responses (e.g. mooring line tension, pitch, surge, or heave) in a floating offshore structure. CWEs are naturally occurring events extracted from simulated or measured sea-states, capturing the non-linear interactions and dynamic features responsible for extreme loading conditions.

Hyper-Group: A synthetic, short-duration wave event composed of multiple focused wave groups. Each group is deterministically described by its spectrum, phase, and temporal location within the HG. Since the HG is a linear superposition of these groups, it also represents a linear surface elevation.

Design Hyper-Group: A probabilistically generated Hyper-Group designed to replicate the effects of CWEs on floating offshore structures under specific sea-state conditions. DHGs are derived from a stochastic framework developed through the analysis of hundreds of CWEs.

The properties of a DHG's components are conditionally sampled based on sea-state features and natural periods of the floating structure. A DHG is tailored to induce a specific extreme response (e.g. mooring line tension, pitch, or heave) and carries a specified probability of occurrence and a probability of exceedance for induced response thresholds, which are defined during the development of the stochastic framework. The technical details of this probabilistic framework, including how the calculated statistics are processed to generate DHGs, are beyond the scope of this paper and will be addressed in future work.

Within the context of this work, CWEs specifically concern extreme mooring line tension response. They are identified and isolated from fully non-linear sea-state realisations using envelope analysis to define their temporal boundaries and characteristics. Having clarified the distinctions between 'critical wave event', 'Hyper-Group' and 'Design Hyper-Group', it is now possible to state the purpose and scope of this work.

The primary objective is to demonstrate how the application of amplitude correction and phase focusing techniques to HGs propagated in a non-linear environment by extension enables the practical application of DHGs in design analyses for floating offshore wind turbines (FOWTs). The key advantage of HGs lies in their deterministic composition: each HG consists of a finite number of FWGs, for which the spectrum, phase, and temporal location are defined a priori. This structure enables precise reproduction of the entire HG in numerical or experimental wave tanks, avoiding the challenges associated with correcting and focusing actual CWEs (i.e. those extracted from measured or simulated long surface elevations). Overall, this approach provides a computationally efficient alternative to long-duration sea-state simulations, enabling targeted testing of offshore structures under extreme conditions.

A secondary objective is to assess and enhance the physical realism of DHGs when subjected to non-linear wave propagation. While DHGs are synthetically generated to replicate extreme structural responses, their realism under conditions where wave–wave interactions alter wave dynamics must be validated. This is addressed through the same process applied for the primary objective, where finally a new, 'realistic' linear component of the corrected Hyper-Group (CHG) is obtained through spectral decomposition and harmonic separation. This component can then be integrated into multi-physics tools like OpenFAST, where second-order effects are added via closed-form schemes. By doing so, it is ensured that the synthetic wave events used in structural analyses are not only energetically consistent but also physically representative of real-world hydrodynamics.

The proposed process is demonstrated in a numerical wave tank, using the fully non-linear potential flow solver OceanWave3D of Engsig-Karup *et al*. (2009), following a simplified approach detailed in Section 2. Section 3 presents the application of the methodology of Gaussian regression and reconstruction as an HG to a single CWE for mooring line tension, rather than directly using a synthetic DHG. Then, the iterative amplitude correction and phase focusing process is applied to each individual FWG composing the obtained HG, exactly as it would be applied to a DHG. Following the convergence of the correction process for each individual FWG, they are recombined as a CHG and propagated in the numerical wave tank. The resulting CHG is used as input for an OpenFAST FOWT model, and the induced mooring line tension is compared to that of the original CWE, its initial HG representation (pre-correction) and the sea-state section from which the CWE was isolated. The results demonstrate a high level of agreement compared to the original CWE and the importance of non-linear propagation in making a synthetic DHG more realistic.

2. Materials and methods

The process for the reproduction of CWEs involves the generation of fully non-linear sea-state realisations, wave–structure interaction simulations, envelope analysis via Hilbert transform and isolation of CWEs, the generation of a corresponding HG composed by FWGs, and finally the reproduction of the HG in a numerical wave tank via amplitude correction and phase focusing of the individual FWGs.

2.1 Sea-state realisations and OceanWave3D simulations

A wave scatter diagram is considered, representative of potential floating offshore wind farm locations in the Mediterranean sea. Random sea-state realisations are defined based on a JONSWAP spectrum, for a number of significant wave height H_s and peak wave period T_p pairs. The sea-state cases are selected based on three main considerations: first, to represent a range of extreme conditions; second, to cover a spectrum of significant steepness values; and third, to avoid wave breaking, which imposes a constraint on the maximum steepness of the selected sea-states. Extreme conditions are defined here as sea-states with return periods exceeding one year and relatively long peak wave periods. The rationale for these choices is rooted in the observation that CWEs for mooring line tension can also occur in more frequently occurring sea-states, with their effects naturally becoming more pronounced when the peak wave period approaches the natural periods of the FOWT.

The sea-states are propagated using the OceanWave3D fully non-linear potential flow solver, resulting in a vast set of free surface elevations and wave kinematics. Then, the spectral decomposition and separation of harmonics of the surface elevations allows the isolation of the linear component to be used for the next steps.

The datasets are generated starting from seven different cases of sea-state parameter combinations. Each case is labelled based on the parameters of the initial JONSWAP spectrum which was then utilised for the fully non-linear propagation via OceanWave3D. Thus, the cases are noted by H_s^J and T_p^J pairs, referring to the initial linear realisation of the JONSWAP spectrum that was used as input. For each case (H_s^J, T_p^J pair), 20 different sea-states (different randomly distributed phase angles) were realised in OceanWave3D, leading to a total of 140 fully non-linear sea-states. Naturally, due to non-linear wave–wave interactions, the resulting significant wave height H_s is lower than the H_s^J defining the initial JONSWAP spectrum; meanwhile, the resulting T_p will also show some variation compared to T_p^J.

Table 1 summarises the cases for the sea-state simulations along with the median values for the significant wave height, peak wave period, and significant sea-state steepness which is defined as:

Table 1. Summary of statistics from OceanWave3D simulations

Case	H_s^J: m	T_p^J: s	$(H_s)_{50^{th}}$: m	$(T_p)_{50^{th}}$: s	$(\varepsilon_{ss})_{50^{th}} \times 10^{-2}$
1	5.0	8.0	4.624	8.032	4.59
2	6.0	8.0	5.338	7.913	5.45
3	6.0	10.0	5.770	10.058	3.65
4	7.0	10.0	6.618	9.942	4.29
5	8.0	10.0	7.445	9.948	4.80
6	7.0	12.0	6.817	11.916	3.07
7	8.0	12.0	7.744	11.796	3.55

1. $$\epsilon_{ss} = \frac{2\pi}{g}\frac{H_s}{T_p^2}$$

Starting from the rule-of-thumb, 3-h interval for statistical stationarity of a sea-state, the length of the simulations is defined as 2 raised to an integer power $\lceil log_2(3 \times 3600) \rceil$. Therefore, the duration of each sea-state realisation is $t_e = 2^{13} = 8192$ [s] ($\approx 2\frac{1}{4}$ [hr]).

A sensitivity analysis was conducted in OceanWave3D to evaluate the impact of spatial and temporal discretisation on the accuracy of wave simulations. Four cases were tested using a challenging sea-state condition (H_s = 8 [m], T_p = 12 [s]), where the coarsest resolution was constrained by the Courant number condition ($Cr \leq 1$) for the lowest frequency components of the discretised JONSWAP spectrum. The results are presented in Table 2, where $Cr(f_p)$ is the Courant number at the peak wave frequency, Δt is the time step, Δx is the spatial resolution, N_z is the number of vertical grid points, E is the spectral energy, and var, skew, and kurt refer to the variance, skewness, and excess kurtosis of the surface elevation, respectively.

The 'Coarser' discretisation was selected for this study (Cr = 0.633, $\Delta t = 2^{-3}$) due to its optimal balance between accuracy and computational efficiency. Compared to the 'Baseline' case, it exhibits only a 0.36% reduction in significant wave height and a 0.72% decrease in spectral energy (E), while preserving higher-order statistics (e.g. skewness and kurtosis). These metrics confirm that the dominant wave dynamics, critical for low-frequency structural responses such as mooring line tension, are accurately captured. In addition, the reduced computational demand enables practical application in iterative correction processes and long-duration simulations.

In the context of the discretisation of the computational domain, the seven cases can be categorised in three groups based on the peak wave period (I,II,II $\equiv T_p = 8, 10, 12$ [s]). The basic

Table 2. Convergence study for OceanWave3D discretisation parameters

Case	$Cr(f_p)$	Δt: s	Δx: m	N_z	H_s: m	ΔH_s: %	E	ΔE: %	Var	Skew	Kurt
Baseline	0.509	2^{-4}	2.3	23	7.812	0.0	58.494	0.0	3.814	0.156	−2.982
Coarser	0.633	2^{-3}	3.7	15	7.784	−0.36	58.072	−0.72	3.787	0.164	−2.986
Coarse	0.325	2^{-4}	3.7	15	7.791	−0.27	58.187	−0.52	3.795	0.153	−3.002
Fine	0.616	2^{-4}	1.9	27	7.813	+0.01	58.503	+0.02	3.814	0.151	−2.987

parameters of the spatio-temporal discretisation are summarised in Table 3.

For the discretisation of the input JONSWAP spectrum, the frequency interval is defined by the duration of the simulation as $\Delta f = 1/t_e$. Given the range of wave heights $H_s \in [5, 8]$ used in the simulations and considering the recommendation in DNV (2010), a first approximation of the cut-off frequency is obtained via the expression $f_{cut} = (2\pi)^{-1}\sqrt{2g/H_s} \approx 0.25 : 0.32$. The number of frequencies N_s was defined as 2 raised to an integer power $\lceil log_2[(f_{cut} - f_{min})/\Delta f]\rceil$, by considering the frequency range to be 2 raised to a negative integer power, specifically $f_{cut} - f_{min} = 2^{-1}$.

Table 3. Discretisation of computational domain

Group	N_x	N_z	Δx: m	L: m	d: m	f_s: Hz	Δt: s	N_t
I	801	21	2.5	—	—	—	—	—
II	646	17	3.1	2000	100	2^3	2^{-3}	2^{16}
III	542	15	3.7	—	—	—	—	—

Table 4. Discretisation of the JONSWAP spectrum

Δf: Hz	N_s	f_{min}: Hz	f_{cut}: Hz	$max(\kappa d)$
2^{-13}	2^{12}	2^{-5}	$\frac{17}{32}$	113.577

The values for the discretisation of the frequency domain are presented in Table 4.

The JONSWAP wave spectrum with peakedness factor $\gamma = 3.3$ is utilised for the generation of irregular waves imposed as boundary conditions at the western boundary of the numerical wave tank. The total wave system is obtained as

$$\eta(t) = \sum_{i=1}^{N_s} \hat{\eta}_i \cos(-\omega_i t + \phi_i) \quad (2)$$

where the component amplitude is defined as $\hat{\eta}_i = \sqrt{2S(\omega_i)\delta\omega}$ and the phase angle is random, calculated as $\phi = \angle a + ib$ where $a,\ b \in \mathcal{N}(0, 1)$ (normal distribution).

Figure 1 illustrates the geometry of the computational domain defined in OceanWave3D along with the position of the probes where the surface elevation and other wave kinematics are recorded. Probe 0 corresponds to the position of the wavemaker, while Probe 3 is the phase focus location where the measured surface elevation is the input for the wave–structure interaction simulations following the required processing. The generation and absorption (relaxation) zones are set up to both have lengths of $\lambda_{max}/2$, where λ_{max} is the maximum wavelength, corresponding to

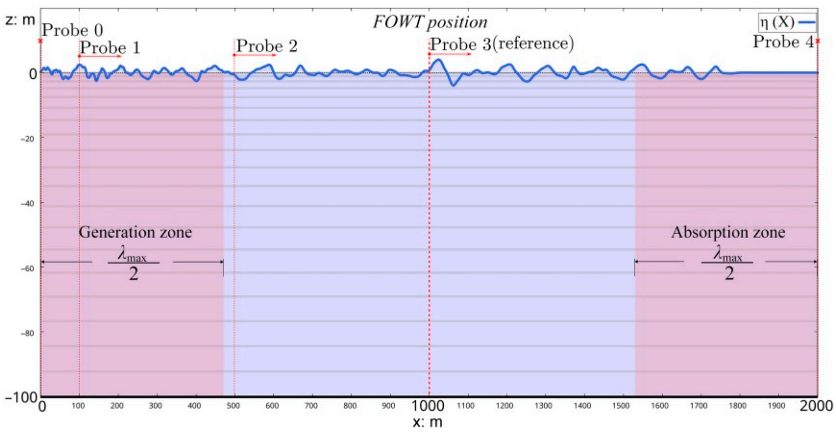

Figure 1. Computational domain in OceanWave3D

the minimum frequency defined in the discretisation of the input JONSWAP spectrum.

Only unidirectional waves are considered as the most critical loading conditions for mooring systems often arise from unidirectional wave groups aligned with the 'down-wave' mooring line. This assumption is both appropriate and conservative for assessing maximum expected tension levels under given metocean conditions. While directional spreading can influence the spatial and temporal focusing of wave energy, the core methodology presented in this work (amplitude correction, phase focusing, and iterative correction of HGs) is independent of the directional characteristics of the sea-state. Extending the methodology to multi-directional sea-states would primarily involve enhancing the probabilistic framework for generating DHGs, which is a subject for future work.

Regarding wave-breaking effects, investigating their applicability requires a different set of computational tools such as CFD simulations, or purely experimental testing in physical wave tanks to fully capture the associated highly non-linear dynamics. However, this work focuses on demonstrating how the underlying linear framework of the proposed methodology enables computationally efficient reproduction of CWEs in a controlled, non-breaking environment. The non-breaking condition is imposed using a $0.5\,g$ limit for the vertical particle acceleration, whereas the solver applies smoothing at the instances where this limit is violated. It was ensured through the steepness of the sea-state cases selected that the required smoothing corrections are very rare as to not affect the results in any significant way.

Next, using the method of harmonic separation described in Fitzgerald *et al*. (2014), decomposition of each sea-state realisation up to the fourth order is achieved using each set of four resulting non-linear surface elevations from OceanWave3D in order to isolate the first-order (linear) component of the propagated sea-state.

For each case of $(H_s,\ T_p)$ pair, a numerical sea-state is generated as in Equation 2 using a random phase angle ϕ. This is considered as the reference or 'ϕ_0' realisation. Then, three additional realisations are generated corresponding to the necessary phase shifts $\phi_0 + \pi/2,\ \phi_0 + \pi,\ \phi_0 + 3\pi/2$. The four surface elevations are then passed to OW3D as boundary conditions for the non-linear propagation. The results are four non-linear signals that allow the application of the four-wave harmonic separation method and subsequent spectral decomposition.

The Fourier transforms of the four surface elevations are denoted by s_0, s_1, s_2, s_3 accordingly. The phase angles are 'synchronised', so that $\phi = 0$ at the peak wave frequency $f_p = 1/T_p$ for all four signals. This is achieved by calculating and adding the required number of phase corrections. Finally the spectra of the linear, difference-frequency, sum-frequency, and third-order components are obtained as

3. $$S_1 = (s_0 - is_1 - s_2 + is_3)/4$$

4. $$S_{2^-} = (s_0 + s_1 + s_2 + s_3)/4$$

5. $$S_{2^+} = (s_0 - s_1 + s_2 - s_3)/4$$

6. $$S_3 = (s_0 + is_1 - s_2 - is_3)/4$$

The corresponding surface elevations $\eta_1(t),\ \eta_{2^-}(t),\ \eta_{2^+}(t),\ \eta_3(t)$ are then obtained via the inverse Fourier transform of each spectrum accordingly.

2.2 OpenFAST model and simulations

A numerical model of a FOWT defined in the non-linear aero-hydro-servo-elastic simulation tool OpenFAST is utilised to carry out time-domain simulations given the generated sea-states as inputs. The response of the FOWT is analysed, allowing the identification of extreme response events in the various degrees of freedom. For this work, the focus is primarily on the analysis of extreme mooring line tension events.

The 140 sea-states were then used as input to the OpenFAST software package to calculate the response of the FOWT, identify extreme responses of mooring line tension, and isolate the corresponding CWEs within the sea states. Utilising the first-order surface elevation obtained from the four-wave decomposition as input, the equations of motion of the modelled structure are solved in the time and frequency domains. This results in the response of the FOWT in all degrees of freedom along with mooring line loads up to the second order (Alonso Reig *et al*., 2023).

Within OpenFAST, second-order waves are modelled using sum and difference frequency interactions between pairs of first-order wave components. This scheme employs the transfer function derived by Sharma and Dean (1981). The frequency ranges for difference and sum interactions are defined as $[0, f_p]$ Hz for difference frequencies and $[f_p,\ f_{cut}]$ Hz for sum frequencies. The chosen ranges ensure that the energetic content of the second-order wave forces is accurately captured while maintaining computational efficiency. The second-order floating platform forces are computed using the full QTF of the difference and sum frequencies.

The FOWT computational model employed in the entirety of the analysis is the DeepCwind floating wind system with a semi-submersible substructure combined with NREL's offshore 5 MW baseline wind turbine, defined in Robertson *et al*. (2014) and experimentally validated in Robertson *et al*. (2017). The only changes made to the original DeepCwind OpenFAST model were related to the mooring system. In particular, the depth of the seabed was considered to be 100 m during this work in order to accommodate a related experimental campaign by Paradeisiotis *et al*. (2025) with a scaled model of a similar FOWT concept. Therefore, the change of depth for the OpenFAST simulations, made the adjustment of the mooring line length necessary to adapt to the lower depth. This in turn means that the weight of the mooring lines is also different, thus, the platform mass (i.e. ballast) also had to be slightly adjusted to maintain the same draught at the equilibrium position of the FOWT.

In comparison to the original FOWT system as defined in OpenFAST, these modifications resulted in a 10% reduction in the surge natural period (from 113.764 [s] to 102.388 [s]), indicating a slightly stiffer system in the surge direction, while the pitch and heave natural periods remained unchanged. This adjustment does not affect the general applicability of the methodology for reproducing CWEs or HGs. It is important to distinguish between the probabilistic framework for generating DHGs and the general reproduction process of HGs demonstrated in this work. While the probabilistic framework, which is developed based on a specific FOWT configuration, incorporates non-dimensional parameters (e.g. correlations with structural natural periods) to facilitate future generalisation, its transferability to other FOWT designs requires further investigation. In contrast, the reproduction methodology itself (amplitude correction, phase focusing, and recombination) is general and independent of the specific structural configuration or water depth.

2.3 Identification of critical wave events

To classify which wave events are critical, it is required to define what constitutes an extreme response event within each sea-state/structure interaction simulation. Therefore, threshold values are calculated for each variable of interest. Specifically, the response peaks from the time history of each variable which are higher than the root-mean-squared (rms) value ($y(t_i) > y_{rms}$) are considered and the following dimensionless quantity is defined:

7. $$\bar{y}_{rms} = \frac{y(t_i)}{y_{rms}} - 1$$

Thus, a dataset is created from this quantity from all the qualified peaks, which is then fitted by an appropriate statistical distribution. This is a classic problem in extreme value theory, where the choice of distribution depends on the tail behaviour of the dataset and the physical processes driving the corresponding extremes values. The generalised extreme value distribution framework is employed, which nests the Gumbel, Weibull, and Frèchet distributions as special cases. Finally, the threshold of extreme response for each variable is defined by the top 1% of peaks via the quantile function of the corresponding distribution $Q(p = 0.99)$.

Having identified the response peaks that qualify as extreme, the corresponding instance in the exciting surface elevation is associated. Next, it is necessary to define the extent of the corresponding CWE around the associated instance, to isolate its surface elevation for further processing and recreation. Given the surface elevation $\eta(t)$ of the sea-state, through the Hilbert transform $\mathcal{H}\{\eta(t)\}$ the envelope $u(t) = |\mathcal{H}\{\eta(t)\}|$ and instantaneous phase angle $\theta(t) = \angle\mathcal{H}\{\eta(t)\}$ are obtained. Thus, the surface elevation is expressed exactly as $\eta(t) = u(t)e^{i\theta(t)}$.

The duration of the wave event ΔT_{ev} is selected based on the instantaneous frequency $\omega_{\mathcal{H}} = \frac{d\theta}{dt}$. The limits of the wave event are defined by the discontinuities of instantaneous frequency prior and after the instance of the extreme response. Discontinuities here are defined as the time instances where the value of instantaneous frequency is zero or negative ($\omega_{\mathcal{H}} \leq 0$). Finally, the immediate prior and posterior zero-crossing in the surface elevation are used as the lower and upper limit of a wave event.

2.4 Reproduction of critical wave events

To allow for the systematic statistical processing of CWEs and to aid the recreation process of individual wave events, a characteristic angular frequency $\tilde{\omega}$ of the wave event and a constant phase angle $\tilde{\phi}$ are defined. This is done by approximating the instantaneous phase $\theta(t)$ of the isolated wave event by a linear regression function as

8. $$\text{unwrap}\{\theta(t)\} \approx \tilde{\omega}t + \tilde{\phi}$$

At this stage, the methodology of Stagonas and Paradeisiotis (2025) is employed to express the CWE as a combination of FWGs that is a HG. Technical details of this methodology are beyond the scope of this work; however, for the purposes of completeness, a brief summary is provided. This process involves the regression of a wave event's envelope as the sum of N Gaussian elementary envelopes:

9. $$u(t) \approx G(t) = \sum_{n=1}^{N} g_n(t)$$

where

10. $$g_n(t) = A_n \exp\left[-\left(\frac{t - t_n^c}{T_n}\right)^2\right]$$

For each isolated CWE, the surface elevation time history is shifted so that the instance of the extreme response coincides with $t = 0$. Hilbert transform is applied again to obtain the analytic signal of the CWE and consequently calculate its envelope and instantaneous phase angle. The number of Gaussian functions, N, used to approximate the envelope of a CWE, depends on the number of local maxima M in the original envelope $u(t)$. To identify these maxima, a low-pass filter with a cut-off frequency of $f_{cut}/2$ is first applied to $u(t)$. A constraint is then imposed to ensure that the temporal distance between consecutive peaks exceeds $2/f_{cut}$, thereby avoiding closely spaced peaks that could impede convergence. If this constraint is violated, only the peak with the larger amplitude is retained.

The Gaussian regression algorithm then determines the optimal characteristic widths T_n of the Gaussian functions $g_n(t)$, with initial conditions based on the second time-derivative of the remaining peaks. This is formulated as a least squares minimisation problem, with a constraint $0 < T_n < 1/f_{min}$ applied to ensure physically meaningful results. Gaussian functions for which $T_n \to 0$ are discarded. This process results in a set of $N \leq M$ Gaussian elementary envelopes, each characterised by a triplet of parameters $\{A_n, T_n, t_n^c\}$.

The iterative optimisation for Gaussian envelope regression terminates when either the relative tolerance criterion ($\epsilon \leq 10^{-5}$) is met for the T_n values of all elementary envelopes or the maximum iteration limit (10^4) is reached. This ensures robust convergence, with $\approx$9% of regressions reaching the iteration cap due to minor numerical oscillations near boundary conditions (e.g. $T_n \to 0$). Such cases do not indicate failure but reflect the maximum achievable accuracy within the computational constraints. Further technical details, including the objective function and numerical integration scheme, are provided in Stagonas and Paradeisiotis (2025).

Next, the HG is obtained as the sum of N FWGs, each corresponding to a Gaussian elementary envelope. The *nth* FWG is generated as

11. $$\eta_n(t) = \frac{A_n}{\sum P_n \Delta f} \sum_{i=1}^{N_f} P_n(f_i) \Delta f \cos[-\omega_i(t - t_n^c) + \phi_n]$$

using a corresponding variance spectrum

12. $$P_n(f) = \frac{1}{2} \frac{|S_n(f)|^2}{\Delta f}$$

By using the characteristic frequency $\tilde{\omega}$ from Equation 8, the amplitude modulation of a unit amplitude wave with frequency $\tilde{\omega}$ by each nth Gaussian elementary envelope

13. $$\eta_{g_n} = g_n(t) e^{-i\tilde{\omega}t}$$

provides the amplitude spectrum as $S_n(f) = \mathcal{F}\{\eta_{g_n}\}$. Lastly, the phase angle ϕ_n is calculated as $\phi_n = \tilde{\phi} - \theta(t_n^c) - 2\pi/T_n t^c$.

While the Gaussian regression and HG generation process is designed for statistical processing of CWEs to build a probabilistic framework for DHGs, this work demonstrates its application to a single CWE as a proof of concept. The goal is not high-fidelity reconstruction of individual CWEs but illustration of how the same technical steps (correction, focusing and recombination) apply to both CWEs and DHGs. The probabilistic robustness of DHGs is acknowledged but not explored here; instead, the focus is on validating the core process of amplitude correction and phase focusing in a controlled setting. The accuracy of reproduction for a single CWE depends on the initial envelope regression, but the methodology's broader applicability to synthetic DHGs remains its primary advantage.

Finally, to correctly generate waves of a pre-selected target spectrum, the iterative procedure of Buldakov *et al*. (2017) is followed to calculate the required amplitude and phase corrections:

14. $$a_{in}^n(f_i) = a_{in}^{n-1}(f_i) \frac{a_t(f_i)}{a_{out}^{n-1}(f_i)}$$

15. $$\phi_{in}^n(f_i) = \phi_{in}^{n-1}(f_i) + [\phi_t(f_i) - \phi_{out}^{n-1}(f_i)]$$

where a_{in} is the input amplitude spectrum, a_t the target amplitude spectrum, a_{out} a recorded output spectrum and ϕ the phase of a spectral component. The a_{out} amplitude spectrum, does not necessarily correspond to the focus location. In fact, it is preferable to be placed close to the wavemaker in certain cases. Further, discussion regarding selection of the amplitude correction location, follows during the presentation of the results in the next section.

Beginning with the separated, first-order component of the surface elevation of an identified CWE, $\eta(t)$, the one-sided amplitude spectrum and phase are computed using a fast Fourier transform (FFT). The target amplitude spectrum a_t and phase angle ϕ_t at the focus location are defined by evaluating B-spline interpolations applied to the original amplitude spectrum, and unwrapped phase within the frequency limits f_{min} and f_{cut} as defined in the full sea-state simulations (Table 4), ensuring smooth transitions and consistent frequency resolution. To further assist the correction and focusing process, a low-pass filter with a cut-off frequency of $3f_p$ is applied to the amplitude spectra of the individual FWGs. This filtering removes high-frequency spectral components without compromising the energetic content of the FWGs.

The length of the CWE, HG and individual FWG simulations, is defined as 2 raised to the integer power of $\lceil log_2(2L_{dom}/\upsilon_{min})\rceil$ where υ is the wave celerity, namely, based on the time required for the slowest wave (corresponding to f_{cut}) to make a round trip to the western boundary of the computational domain. Prior to the calculation of the required phase shift for the wavemaker signal, the target surface elevation (focus location) is shifted in time by L_{dom}/υ_{min}, to allow proper mixing and for all the frequency components to be correctly propagated.

Then, the surface elevation at the focus location $\eta_f(t)$ is reconstructed by superposing the individual frequency components:

16. $$\eta_f(t) = \sum_{j=1}^{N_s} a_{t,j}\cos(\omega_j t + \phi_{t,j})$$

The wavemaker signal is generated by correcting the phase of each frequency component to account for propagation from the wavemaker location x_0 to the focus location x_f. The wavenumber κ for each frequency component is calculated using the dispersion relation $\kappa = \kappa_0 \coth(kd)$, where $\kappa_0 = \omega^2/g$ is the deep water wavenumber. The phase correction $\Delta\phi$ is then calculated as $\Delta\phi = \kappa(x_f - x_0)$, therefore, the phase at the wavemaker comes as $\phi_{wm} = \phi_t + \Delta\phi$. The surface elevation at the wavemaker $\eta_{wm}(t)$ is generated by superposing the corrected phase components:

17. $$\eta_{wm}(t) = \sum_{j=1}^{N_s} a_{wm,j}\cos(\omega_j t + \phi_{wm,j})$$

where the amplitudes a_{wm} are the same as the target amplitudes a_t for the initial calculation. For subsequent correction iterations, the input spectrum a_{in} for the wavemaker is calculated from Equation 14 and $a_{wm} = a_{in}$ is set for the calculation of the wavemaker signals from Equation 17. To enable the harmonic separation and spectral decomposition process, three additional wavemaker signals with phase shifts of $\pi/2$, π and $3\pi/2$ relative to $\eta_{wm}(t)$ are generated for propagation.

Four convergence metrics are employed to govern and evaluate the iterative amplitude and phase correction process for each FWG, by comparing each correction iteration (C0,C1,C2,…) to the target. These metrics include the percentage difference in maximum wave height (ΔH_{max}), the cosine similarity (CS_t) of the temporal surface elevation, the normalised mean squared error ($NMSE_s$) of the amplitude spectrum and the percentage difference in phase angle at the peak frequency ($\Delta\phi(f_p)$). Convergence was deemed achieved when $\Delta H_{max} < 3\%$, CS_t approached unity (typically >0.95), $NMSE_s$ approached zero (typically <0.05), and $\Delta\phi(f_p)$ approached zero (typically $<2\%$).

These thresholds are selected based on their physical significance in capturing the dynamic behaviour of the FWGs. A ΔH_{max} error below 3% ensures that the peak wave height, which is critical for loading conditions, is accurately reproduced. The CS_t guarantees that the corrected temporal shape aligns with the target, preserving the essential focusing characteristics. The $NMSE_s$ ensures that the spectral energy distribution remains consistent with the target. Finally, $\Delta\phi(f_p)$ is used to maintain phase alignment at the dominant frequency.

3. Results and discussion

The proposed approach to improve the accuracy in the reproduction of CWEs, that is, wave events that often include steep wave groups, is demonstrated in the following results produced in the numerical wave tank setup using the fully non-linear wave propagation code OceanWave3D. This demonstration is carried out for a specific CWE which belongs in case 3 ($H_s^J = 6.0$ m, $T_p = 10$ s). The duration of each simulation is t_e = 2048 [s] with Δt = 0.125 [s] and the target a_t and input a_{in} spectra contain $N_s = 512$ frequency components for $f \in [f_{min}, f_{cut}]$. The spatial resolution of the computational domain was also redefined, with Δx = 2.7 [m], N_x = 742 and N_z = 20.

First presented are the results for the conventional approach of amplitude correction and phase focusing, namely, using as targets the amplitude spectrum and phase angle of the first-order (linear) component of the entire CWE. This aims to highlight the challenges when trying to reproduce such a complex and steep wave event, while it serves as a reference point to illustrate the efficacy of the proposed approach. Next, the second set of results concern the corresponding Hyper-Group, obtained through the process of Gaussian envelope regression and reconstruction with FWGs. In that, the amplitude correction and phase focusing is individually applied to each composing FWG. Then, the individual corrected spectral quantities are combined to reproduce a corrected version of the entire Hyper-Group (CHG). Finally, the two sets of results are compared both in terms of the corrected surface elevations and most importantly regarding the induced mooring line tension in the FOWT model in OpenFAST.

3.1 Wave event reproduction

The first step in each cycle of propagation in either a numerical or experimental wave tank and subsequent amplitude correction and phase focusing is the harmonic separation and spectral decomposition of the wave event. This allows the isolation of the first-order (linear) component of the waves upon which the correction and focusing is applied and the corrected first-order component is propagated for the next iteration.

Figure 2 illustrates the resulting amplitude spectra and phase angles of the 1st, 2nd$^-$, 2nd$^+$ and 3rd order components along the corresponding amplitude spectrum $A(\eta)$ and phase angle of the examined CWE. This illustration highlights the transfer of energy to lower and higher frequencies relative to the peak wave frequency due to non-linear wave–wave interactions. In particular, for frequencies $f > 3f_p$ approximately, the amplitude of the first-order component becomes significantly lower than that of the higher order components, indicating that above $3f_p$, the surface elevation is dominated by non-linear effects, while the linear component contributes minimally. This observation supports the later application of the low-pass spectral filter to the target amplitude spectra of individual FWGs during the amplitude correction process. The filter's sole purpose is to prevent numerical instabilities by removing high-frequency components that contribute minimally to the energetic content but could impede convergence.

Figure 3 shows the resulting corrected non-linear surface elevation of the CWE in comparison with the original ('target') non-linear surface elevation. This comparison highlights the main challenges of attempting to reproduce entire wave events, especially when they include steep waves. The corrected wave event η_f – as measured at the phase focusing location – is the result of five amplitude correction and phase focusing iterations. The large number of required iterations has to do with the fact that the amplitude correction location was set at $x_{ac} = 100$ m (Probe 1 in Figure 1), namely close to the wavemaker. This means that the a_{out} spectrum in Equation 14 corresponding to the amplitude correction location does not differ significantly from the target amplitude spectrum a_{tgt}. Therefore, the amplitude spectrum corrections in each iteration are minor, which slows down the convergence process. However, this choice is necessary because the alternative of selecting the amplitude correction location to be at $x_{ac} \equiv x_f = 1000$ m – or generally closer to the focus location – produces an input amplitude spectrum a_{in} which imposes very sharp corrections due to the complexity of the target spectrum, and leads to the divergence of the iterative correction process.

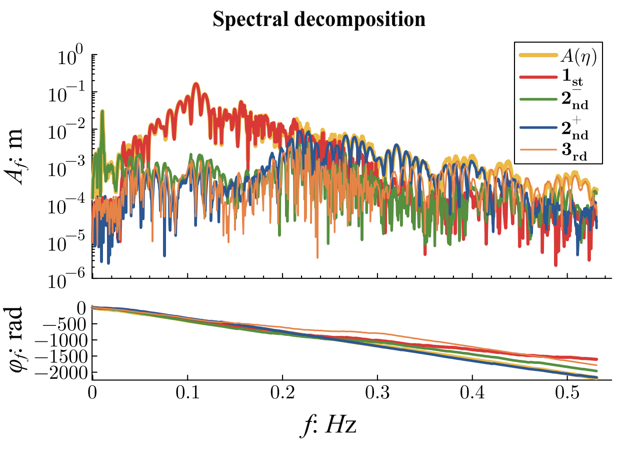

Figure 2. Spectral decomposition of critical wave event

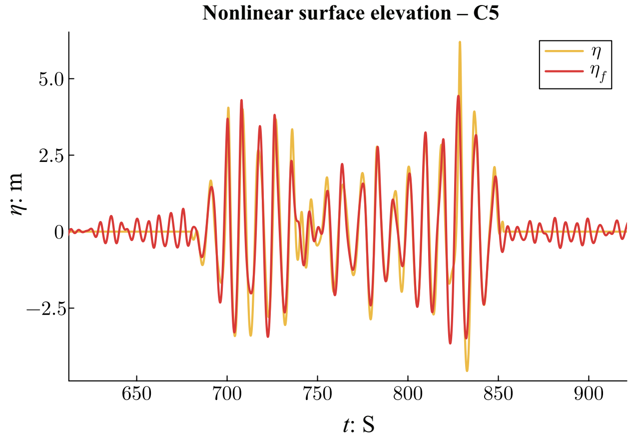

Figure 3. Surface elevation: comparison of original wave event and correction iteration no. 5

A second issue, which is exacerbated by the large number of iterations, is that some frequency components gradually move out of phase and produce waves outside the target time limits of the CWE. Besides the fact that this phenomenon potentially alters the subsequent induced mooring line tension when exciting a floating structure, it leads to the third and main issue, that this 'displacement' of energy carrying components does not allow accurate reproduction of the highest peaks in steep waves where the role of higher-order components is essential. As seen in Figure 3, the difference at the highest peak is significant along with the shape of the dominant wave group at this location which corresponds to the instance of maximum induced mooring line tension in the original CWE. These are the challenges that the proposed approach aims to rectify.

Again, starting from the first-order component of the CWE, a corresponding Hyper-Group composed of 13 FWGs is obtained following the methodology described in Stagonas and Paradeisiotis (2025). The 13 FWGs are enumerated from the highest to the lowest corresponding envelope peak. The amplitude correction and phase focusing iterative process was then applied to each of the 13 FWGs individually. One main difference in the correction process for the FWGs is that, with the exception of the steeper FWG 1, the amplitude correction location was set at the focusing location, that is, $x_{ac} \equiv x_f = 1000$ m. For FWG 1, the amplitude correction location was set at $x_{ac} = 500$ m, namely, at the mid-point of the wavemaker and the focus location. Because the target amplitude spectra of the FWGs are smooth Gaussian curves, convergence of the correction process is much faster. Moreover, the potential impact of the $3f_p$ low-pass filter was quantified by comparing the spectral energy of each FWG before and after its application. The average relative difference in spectral energy for the most energetic FWGs (1–6) was −0.013% which is negligible. Meanwhile, the maximum difference, which was −0.865% for FWG 7, remains well below the threshold of physical or numerical relevance.

An example of the amplitude and phase correction applied in each iteration for the FWGs is presented in Figure 4. The notation ‘C0’ stands for ‘Correction – Number 0’ which corresponds to the initial amplitude correction and phase focusing. It is referred to as ‘initial’ and not first, since no propagation has preceded. Accordingly, ‘C1’, ‘C2’ and so on indicate subsequent correction and focusing iterations, that is, first iteration, second iteration and so on. The convergence behaviour of the iterative correction process for all 13 FWGs is illustrated in Figure 5, which presents the evolution of the four convergence metrics across correction iterations C0–C4. The results demonstrate that most FWGs converge within two to three iterations (C2), meeting all predefined thresholds. However, FWG1, which is the steepest and most non-linear wave group, exhibits slower convergence, with ΔH_{max} and CS_t diverging after C3. The best metrics for FWG1 are observed at C3, beyond which further iterations degrade performance. Similarly, FWG3 requires an additional iteration (C4) to meet the ΔH_{max} and $\Delta\phi(f_p)$ thresholds due to a combination of steepness and phase sensitivity. For all FWGs, the correction process was stopped when further iterations offered diminishing returns, balancing accuracy and computational efficiency.

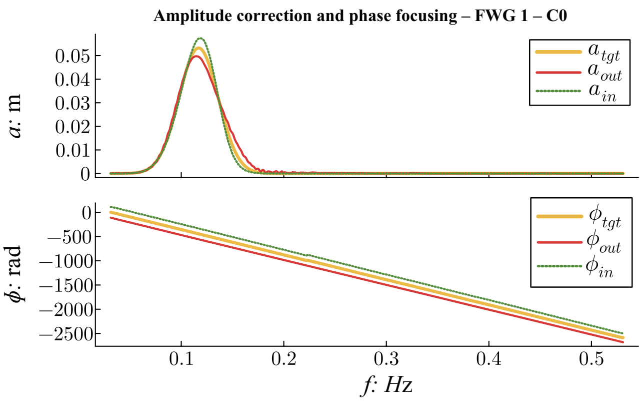

Figure 4. Wavemaker amplitude correction and phase focusing for the generation of a focused wave group in OCW3D

Figure 6 presents the results of the iterative correction process for the first four FWGs. Here, the first-order components of the surface elevation at the focus location (η_f^{1st}) are illustrated against the first-order component of the target FWG from the initial Hyper-Group. For moderately steep FWGs (e.g. FWG 2, FWG 3 and FWG 4), two correction iterations are enough for nearly perfect phase focusing while achieving a deviation of $< 5\%$ in maximum wave height. In contrast, steeper FWGs, such as FWG 1 (top left of Figure 6), present greater challenges due to their increased contribution from higher-order non-linear components. For FWG 1, further correction iterations do not significantly improve amplitude reproduction accuracy, and introduce out-of-focus waves at the start and end of the wave group, similar to the challenges observed when correcting the entire CWE at once. Figure 7 presents the final non-linear surface elevations of all the 13 corrected FWGs to illustrate the temporal location of each within the corrected Hyper-Group. Having now established the corrected input spectrum and phase distribution for each one, it is possible to propagate all FWGs at once to obtain the final CHG.

Since the corrections are applied on the linear components, this means that the wavemaker input is obtained by simple superposition of the individually corrected surface elevations for each FWG. Displayed at the top of Figure 8 is a comparison of the first-order CHG surface elevation (red line) with the initial, target Hyper-Group. Meanwhile, shown at the bottom of Figure 8 is again the first-order CHG surface elevation against the resulting non-linear CHG surface elevation, to highlight the increased amplitude of the highest peaks due to the effects of higher-order wave components. In addition, the resulting non-linear surface elevation of the CHG as propagated in OceanWave3D is displayed in Figure 9 against the original CWE, along with a comparison of the amplitude spectra for the two cases.

Finally, Figure 10 shows the essential comparison of the induced mooring line tension obtained via OpenFAST, between the various cases of exciting waves used in the simulation. The figure shows the response of the upstream mooring line (No. 2) in the direction of the incoming waves. At the top of Figure 10, the red line indicates the response when the full sea-state surface elevation is used as input to the simulation, while the blue line shows the response to the original CWE (not reproduced) which was isolated from this full sea-state’s surface elevation. At the bottom, the full sea-state is used again as reference, while the green line corresponds to the reproduced HG which was derived from the above presented process. For comparison, the initial HG (yellow line) used as the target for the correction is also included.

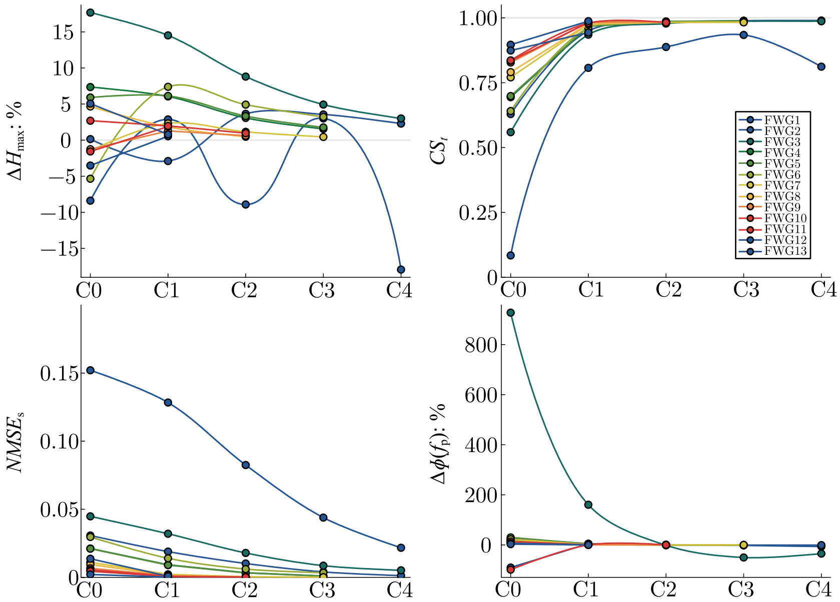

Figure 5. Convergence metrics for the 13 focused wave groups along the correction iterations

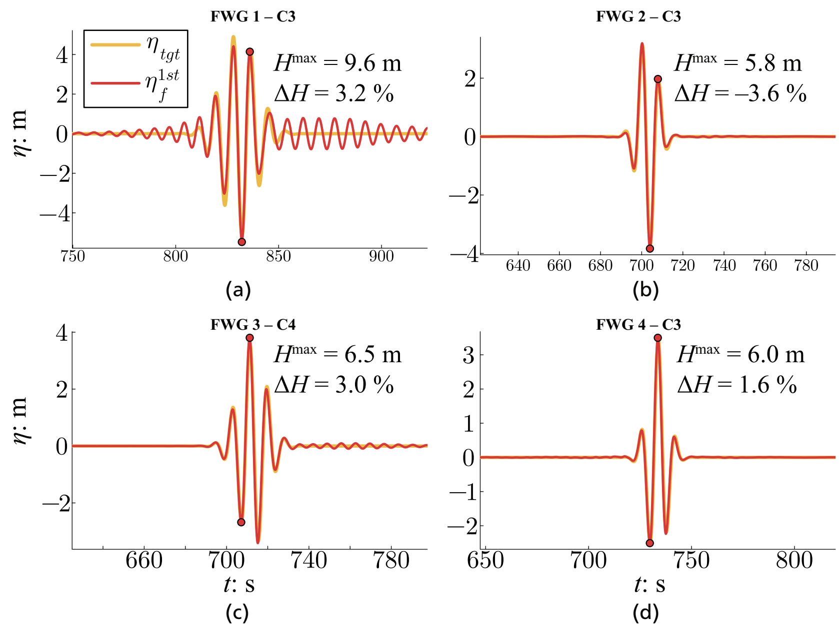

Figure 6. First-order surface elevations: comparison of target and corrected focused wave groups 1–4

Compared to the maximum induced mooring line tension from the full sea-state simulation, the original CWE shows a -1.72% deviation, the initial HG 24.6% and the reproduced HG 4.19%, namely a 20.41% improvement in accuracy between the CHG and the initial HG. This shows that the CHG compares extremely well with the response to the sea-state and the isolated CWE and can be confidently used as an efficient approach to test the FOWT either in a numerical or experimental setting. Furthermore, the impressive improvement in accuracy compared to the initial HG, indicates that the correction and non-linear propagation process serves as a physical refinement mechanism for synthetic HGs. The method accounts for wave–wave interactions, steepening and

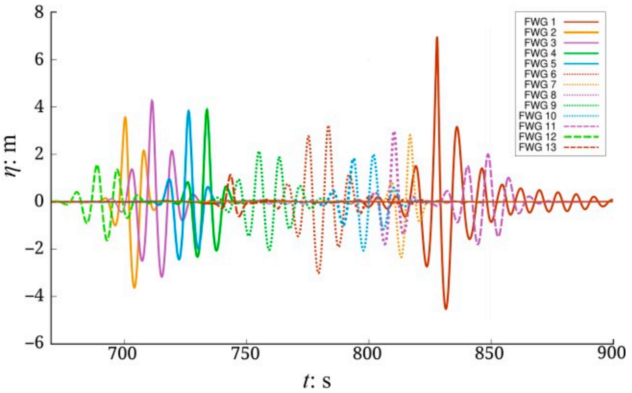

Figure 7. Focused wave groups comprising the corrected Hyper-Group

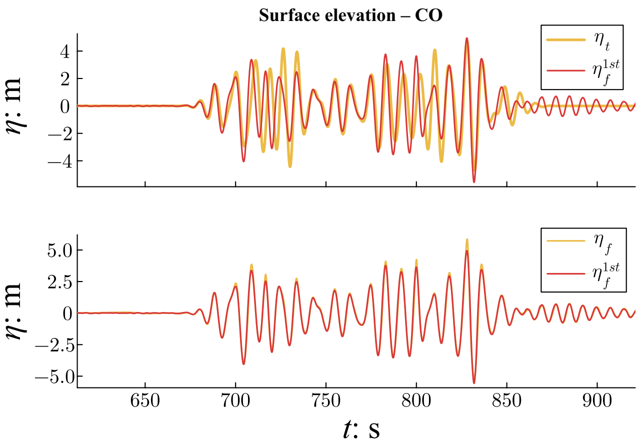

Figure 8. Corrected Hyper-Group surface elevations. Top: Comparison of first-order component with the initial, target Hyper-Group. Bottom: Non-linear corrected Hyper-Group and its first-order component

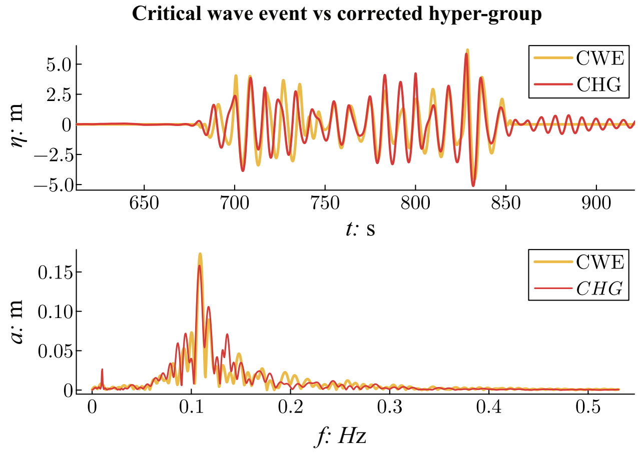

Figure 9. Comparison of the original critical wave event (CWE) with the corrected Hyper-Group (CHG). Top: Non-linear surface elevations. Bottom: Amplitude spectra

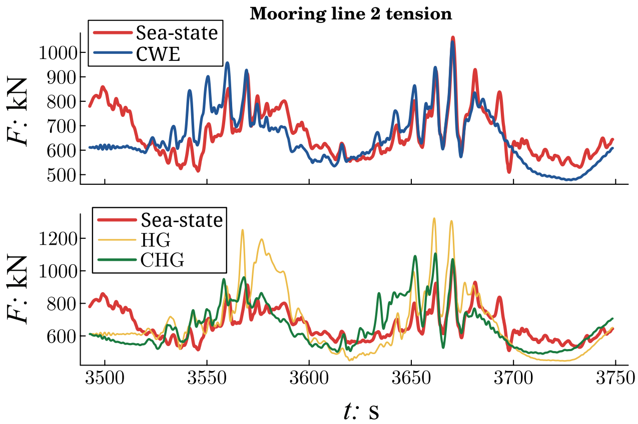

Figure 10. Induced mooring line tension in OpenFAST. Comparison between the full sea-state simulation, the isolated wave event, the initial Hyper-Group and the corrected Hyper-Group

higher-order harmonic generation that are absent in the initial linear superposition. This process effectively filters out non-physical artefacts while enhancing the realism of the surface elevation, ensuring that the corrected HG retains the energetic and focusing characteristics of the CWE.

Overall, when applied to DHGs, the process is highly suitable for experimental model testing, offering precise spatial and temporal focusing of wave energy at the model's location, which is critical for reproducing extreme response conditions (e.g. mooring line tension). The short-duration nature of DHGs reduces experimental time and cost, while their deterministic and linear framework simplifies wave generation using standard wave makers.

However, the methodology faces specific constraints. The Gaussian regression approach to compute an associated HG does not guarantee consistently accurate reconstruction of singular CWEs as the envelope regression accuracy varies on a case-by-case basis. It is instead employed for the development of the probabilistic framework where inaccuracies are averaged out across the large number of processed CWEs, enabling the generation of synthetic DHGs. In addition, very steep waves (near breaking) pose challenges for phase focusing, reducing accuracy in reproducing the highest peaks. Despite these challenges, the presented methodology paired with the concept of DHGs provides a cost-effective and efficient framework for experimental testing while remaining an adequate option for the propagation of singular

CWEs. Future work will focus on refining the methodology for near-breaking waves and refine the envelope regression aspect for CWEs.

4. Conclusions

This study introduces a methodology for identifying and reproducing CWEs that induce extreme responses in floating offshore structures. By isolating the linear component of non-linear sea-states and using the Hilbert transform to define event boundaries, CWEs are systematically extracted and analysed. The recreation process employs iterative amplitude correction and phase focusing, addressing challenges in reproducing steep wave events in numerical and experimental wave tanks. A novel contribution of this work is the decomposition of CWEs into focused wave groups (Hyper-Groups), enabling individual correction and faster convergence. This approach mitigates issues like out-of-phase components and energy displacement, therefore improving the accuracy of reproduction. Validation in OceanWave3D and OpenFAST demonstrates that the CHG reproduces the target event with a 4.19% deviation in induced mooring line tension, closely matching the original CWE and full sea-state response. The methodology provides an efficient framework for testing FOWTs under extreme conditions, reducing computational and experimental costs compared to full sea-state simulations. It enhances the realism of design waves, supporting safer and more reliable offshore structure design. Future work will focus on the experimental validation of this approach in physical wave tanks, conducted in a systematic manner and in conjunction with the probabilistic framework for Design Hyper-Group generation, also enabling the investigation of the applicability range of the underlying linear framework.

Acknowledgements

Andreas Paradeisiotis has received funding from the European Union's Horizon 2020 research and innovation programme under the Marie Sklodowska-Curie Grant Agreement No. 101034403. This work is also part of the project TETHYS (Twinning for excellence in Floating Wind Turbines and Hydrogen Systems – https://www.ucy.ac.cy/tethys/), financed by the Horizon Europe Program of the EU, under contract No. 101159567.

REFERENCES

Adcock TAA, Feng X, Tang T *et al.* (2019) *Application of Phase Decomposition to the Analysis of Random Time Series from Wave Basin Tests*: V009T12A020, 10.1115/OMAE2019-95172.

Aliyar S, Bredmose H, Roenby J, Tomaselli PD and Sarlak H (2025) Directional focused wave group response of a floating wind turbine: harmonic separation in experiments and CFD. *Renewable Energy* **254**: 123516, 10.1016/j.renene.2025.123516.

Alonso Reig M, Pegalajar-Jurado A, Mendikoa I, Petuya V and Bredmose H (2023) Accelerated second-order hydrodynamic load calculation on semi-submersible floaters. *Marine Structures* **90**: 103430, 10.1016/j.marstruc.2023.103430.

American Bureau of Shipping (2020) *Guide for Building and Classing Floating Offshore Wind Turbines 2020. Technical Report*. ABS.

Bennett SS, Hudson DA and Temarel P (2012) A comparison of abnormal wave generation techniques for experimental modelling of abnormal wave-vessel interactions. *Ocean Engineering* **51**: 34–48, 10.1016/j.oceaneng.2012.05.007.

Brown SA, Tosdevin T, Jin S *et al.* (2023) On the selection of design waves for predicting extreme motions of a floating offshore wind turbine. *Ocean Engineering* **290**: 116400, 10.1016/j.oceaneng.2023.116400.

Buldakov E, Stagonas D and Simons R (2017) Extreme wave groups in a wave flume: controlled generation and breaking onset. *Coastal Engineering* **128**: 75–83, 10.1016/J.COASTALENG.2017.08.003.

Cassidy MJ, Taylor RE, Houlsby GT, Eatock Taylor R and Houlsby GT (2001) Analysis of jack-up units using a Constrained NewWave methodology. *Applied Ocean Research* **23(4)**: 221–234, 10.1016/S0141-1187(01)00005-0.

Dermatis A, Bouscasse B, Ducrozet G, Bredmose H and Bingham HB (2025) Prediction of the extreme slow-drift response of moored floating structures using design waves. *Ocean Engineering* **333**: 121456, 10.1016/j.oceaneng.2025.121456.

DNV (2010) *DNV-RP-C205 Environmental Conditions and Environmental Loads*. DNV.

DNV GL (2018) *Class Guideline DNVGL-CG-0130: Wave Loads*. DNV GL, Høvik, Norway.

DNV GL AS (2021) *DNV-ST-0119: Floating Wind Turbine Structures. Technical Report June*. DNV.

Engsig-Karup AP, Bingham HB and Lindberg O (2009) An efficient flexible-order model for 3D nonlinear water waves. *Journal of Computational Physics* **228(6)**: 2100–2118, 10.1016/j.jcp.2008.11.028.

Fitzgerald CJ, Taylor PH, Eatock Taylor R, Grice J and Zang J (2014) Phase manipulation and the harmonic components of ringing forces on a surface-piercing column. *Proceedings of the Royal Society A: Mathematical, Physical and Engineering Sciences* **470(2168)**, 10.1098/rspa.2013.0847.

Fu R, Ma Y, Dong G and Perlin M (2021) A wavelet-based wave group detector and predictor of extreme events over unidirectional sloping bathymetry. *Ocean Engineering* **229**: 108936, 10.1016/j.oceaneng.2021.108936.

Funke ER and Mansard EP (1979) *On the Synthesis of Realistic Sea States in a Laboratory Flume. Technical Report*. National Research Council Canada.

Gudmestad OT, Jonassen TM, Stansberg CT and Papusha AN (2009) Nonlinear one degree of freedom dynamic systems with "burst displacement characteristics" and "burst type response". *In WIT Transactions on the Built Environment* **105**: 299–312, 10.2495/FSI090281.

Hann M, Greaves D, Raby A and Howey B (2018) Use of constrained focused waves to measure extreme loading of a taut moored floating wave energy converter. *Ocean Engineering* **148**: 33–42, 10.1016/j.oceaneng.2017.10.024.

Hansen CL, Bredmose H, Moalemi A *et al.* (2025) Design waves and low-frequency responses of a semi-sub floating wind turbine in spread seas. *Ocean Engineering* **341**: 122682, 10.1016/j.oceaneng.2025.122682.

Hou H-M and Liu Y (2024) An accurate and efficient method to analyze the short-term extreme tension distribution of mooring line under irregular waves. *Ocean Engineering* **304**: 117891, 10.1016/j.oceaneng.2024.117891.

Huang NE, Shen Z and Long SR (1999) A new view of nonlinear water waves: the hilbert spectrum. *Annual Review of Fluid Mechanics* **31(1)**: 417–457, 10.1146/annurev.fluid.31.1.417.

Hudspeth RT and Medina JR (1988) Wave group analysis by the hilbert transform. In *Coastal Engineering Proceedings*. Publ by ASCE, vol. 1, pp. 884–898, 10.9753/icce.v21.66.

Lindgren G (1970) Some properties of a normal process near a local maximum. *The Annals of Mathematical Statistics* **41(6)**: 1870–1883, 10.1214/AOMS/1177696688.

Liu X, Tang T, Mostert W and Adcock TAA (2025) Phase manipulation to analyse different types of nonlinearity using water waves as a case study. *Proceedings of the Royal Society A: Mathematical, Physical and Engineering Sciences* **481**, 10.1098/rspa.2024.0831.

Palfy J (2016) *Guidance Notes on Selecting Design Wave by Long Term Stochastic Method. Technical Report*. American Bureau of Shipping.

Paradeisiotis A, Grande D, Buldakov E, *et al.* (2025) Experimental Validation of a Wave Event Reconstruction Methodology for Floating Offshore Wind Turbines Using Gaussian Elementary Wave Groups, In *35th International Ocean and Polar Engineering Conference (ISOPE)*, OnePetro.

Robertson A, Jonkman J, Masciola M, *et al.* (2014) *Definition of the Semi-Submersible Floating System for Phase II of OC4. Technical Report.* National Renewable Energy Laboratory.

Robertson AN, Wendt F, Jonkman JM *et al.* (2017) OC5 project phase II: Validation of global loads of the DeepCwind floating semisubmersible wind turbine. *In Energy Procedia* **137**: 38–57, 10.1016/j.egypro.2017.10.333.

Senthilkumar R, Romolo A, Fiamma V, Arena F and Murali K (2015) Analysis of wave groups in crossing seas using hilbert huang transformation. In *Procedia Engineering*. Elsevier Ltd, vol. 116, pp. 1042–1049, 10.1016/j.proeng.2015.08.341.

Sharma JN and Dean RG (1981) Second-order directional seas and associated wave forces. *Society of Petroleum Engineers Journal* **21(1)**: 129–140, 10.2118/8584-PA.

Skjoldager Dietz J (2005) *Application of Conditional Waves as Critical Wave Episodes for Extreme Loads on Marine Structures*. Ph.D. thesis, Technical University of Denmark.

Stagonas D, Higuera P and Buldakov E (2018) Simulating breaking focused waves in CFD: methodology for controlled generation of first and second order. *Journal of Waterway, Port, Coastal, and Ocean Engineering* **144(2)**: 06017005, 10.1061/(asce)ww.1943-5460.0000420.

Stagonas D and Paradeisiotis A (2025) A Novel Methodology for the Definition of Design Wave Groups for Offshore Floating Structures, Using Elementary Gaussian Envelopes, In *35th International Ocean and Polar Engineering Conference.* ISOPE.

Tang T, Tromans PS and Adcock TA (2019) Field measurement of nonlinear changes to large gravity wave groups. *Journal of Fluid Mechanics* **873**: 1158–1178, 10.1017/jfm.2019.454.

Taylor PH, Jonathan P and Harland LA (1997) Time domain simulation of jack-up dynamics with the extremes of a Gaussian process. *Journal of Vibration and Acoustics, Transactions of the ASME* **119(4)**: 624–628, 10.1115/1.2889772.

Tromans PS, Anatruk AH and Hagemeijer P (1991) New model for the kinematics of large ocean waves application as a design wave, In *The First International Offshore and Polar Engineering Conference*, ISOPE.

Whittaker CN, Raby AC, Fitzgerald CJ and Taylor PH (2016) The average shape of large waves in the coastal zone. *Coastal Engineering* **114**: 253–264, 10.1016/j.coastaleng.2016.04.009.

How can you contribute?

To discuss this paper, please email up to 500 words to the editor at support@emerald.com. Your contribution will be forwarded to the author(s) for a reply and, if considered appropriate by the editorial board, it will be published as discussion in a future issue of the journal.

Our journals rely entirely on contributions from the civil engineering profession (and allied disciplines). Information about how to submit your paper online is available at www.emeraldgrouppublishing.com/journal/jmaen where you will also find detailed author guidelines.